2021 43rd Annual International Conference of the
IEEE Engineering in Medicine & Biology Society (EMBC)
Oct 31 - Nov 4, 2021. Virtual Conference

Brain network effects related to physical and virtual surgical training revealed by Granger causality

Anil Kamat, Basiel Makled, Jack Norfleet, Xavier Intes, Anirban Dutta and Suvranu De

***Abstract*—this study investigates the difference in effective connectivity among novice medical students trained on physical and virtual simulators to perform the Fundamental laparoscopic surgery (FLS) pattern cutting task (PC). We propose using dynamic spectral Granger causality (GC) in the frequency band of [0.01-0.07]Hz to measure the effect of surgical training on effective brain connectivity. To obtain the dynamics relationship between the cortical regions, we propose to use the short-time Fourier transform (STFT) method. FLS pattern cutting is a complex bimanual task requiring fine motor skills and increased brain activity. With this in mind, we have used high resolution functional near-infrared spectroscopy to leverage its high temporal resolution for capturing the change in hemodynamics (HbO2) in 14 healthy subjects. Analysis of variance (ANOVA) found a statistically significant difference in "LPMC granger causes RPMC" (LPMC→ RPMC) in the subject trained on these two simulator in the first 40 sec of the task. We showed that the directed brain connectivity was affected by the type of surgical simulator used for training the medical students.**

***Key Words*— Fundamental laparoscopic surgery, fNIRS, dynamic Granger causality, Effective connectivity, physical and virtual surgery simulator.**

I. Introduction

SIMULATION-based laparoscopic surgery training has been integrated into the resident program curriculum because it requires a specific set of skills necessary for carrying out surgery. Pattern cutting (PC) is one of the five manual tasks designed by the Fundamentals of Laparoscopic Surgery (FLS) committee to develop hand-eye coordination, visual-spatial perception, and non-dominant hand proficiency. A physical training toolbox is used for the FLS. A virtual basic laparoscopic skill trainer (VBLaST) has been developed to replicate the FLS tasks to overcome well known drawbacks of the physical trainer box [1]. Among these, the virtual simulator is seen as more promising for teaching and assessing performance. Virtual simulators are preferred because they are reusable, do not need consumables and allow more objective quantification of performance. Nevertheless, the metrics used for measuring proficiency are still an active search area for which neuroimaging-based metrics are proposed [2]. Thus, it is essential to compare neuroimaging-based differences between the physical and the virtual simulator (VBLaST) based training.

In this study, we investigated the FLS pattern cutting (PC) task that is a complex bimanual laparoscopic task. Our prior work [2] has established the feasibility of fNIRS technology to measure FLS PC task-related hemodynamic activity at the related cortical regions. The feature that makes this technology suitable for our study is its potential for mobile brain-imaging of subjects without interfering with the surgical training tasks performed in a standard task environment. Prior works have shown that the neurovascular coupling-related fluctuations in the oxyhemoglobin concentration (HbO2) occur in the low-frequency range of [0.01-0.07]Hz [3].

In this study, we investigated neurovascular coupling-related dynamic effective connectivity based on spectral Granger causality. Granger causality is a measure of functional connectivity that can provide the strength and direction of information flow between two simultaneously activated brain regions[4]. Compared to generally used hypothesis-driven causality measurement methods such as structural equation modeling (SEM) and dynamic causal modeling (DCM), GC is a data-driven method for exploring the causal relationships which don't make any *a priori* assumption. This study investigated dynamic effective connectivity based on a sliding window approach to GC [5]. Here, we make a quasistationarity assumption in the sliding window so the window cannot be too long; however, we cannot make it too short for reliable spectral estimates due to the signal's stochastic nature.

Our previous study [2] investigated functional connectivity based on magnitude-squared wavelet coherence. We found the inter-hemispheric functional connectivity between the primary motor cortices to distinguish ($p < 0.05$) the brain network's edge between the physical and the virtual simulators *(under review)*. However, magnitude-squared wavelet coherence did not establish the directionality of the causation\influence between these two regions. Therefore, we used sliding window-based GC to measure directional

The authors would like to gratefully acknowledge funding provided by the Congressionally Directed Medical Research Programs (CDMRP)/ Medical Technologies Enterprise Consortium (MTEC) through fund # W81XWH2090019 with Dr. Darrin Frye as the cognizant program official.

A.Kamat, X.Intes and S.De are with Rensselaer Polytechnic Institute , Troy, NY, USA

A.Dutta is with University at Buffalo, Buffalo, New York, USA

NY,U.S. Army Futures Command, Combat Capabilities Development Command Soldier Center STTC, Orlando FL

brain connectivity.

II. Material and Methods

A. Subjects

The study was approved by the Institutional Review Board of Massachusetts General Hospital, University at Buffalo, and Rensselaer Polytechnic Institute. Fourteen healthy right-handed novice medical students were recruited for the study. Subjects were divided into two cohorts; the physical simulator group (eight subjects) and the virtual simulator group (six subjects). All the subjects were instructed verbally with a standard set of instructions on how to complete the FLS PC task successfully. The optical probes or optodes held by a standard electroencephalography cap (www.easycap.de) were carefully mounted to avoid hairs in between the source/detector and the scalp. During the trial, the subjects were asked to perform the FLS PC task, where the goal was to cut along the circular mark on a piece of gauze as accurately and as quickly as possible. After a baseline rest period of 1min, the trial was started and the maximum time provided for doing the PC task was 5 min.

B. Experimental procedure and measurement

Based on the association of learning a fine motor skill, we identified five functionally specialized brain region, namely left primary motor cortex (LPMC), right primary motor cortex (RPMC), supplementary motor area (SMA), left prefrontal cortex (LPFC), and right prefrontal cortex (RPFC) for observing GC while performing PC task. A 32-channel continuous-wave near-infrared spectrometer (CW6 system, TechEn Inc.) was used that delivered infrared light at 690nm and 830nm. The optode montage consisted of eight long-distance and eight-short distance sources coupled to 16 detectors. 25 long-distance (30-40mm) channels and eight short-distance (~8mm) channels that measured brain activation at preidentifed regions with a sampling frequency of 25Hz.

C. Data Processing

Preprocessing of the raw fNIRS data was kept minimal to reduce misleading results [6]. Motion artifact detection and correction were performed using combined spline interpolation and Savitzky-Golay filtering in HOMER3 (https://github.com/BUNPC/Homer3), which is an open-source software in Matlab (Mathworks Inc., USA). We did not use filtering as it can lead to spurious and missed causalities. Then, modified Beer-Lambert law was used to convert the detectors' raw optical data into optical density. Then, the conversion of optical density to changes in HbO2 concentrations with partial path-length factors of 6.4 (690nm) and 5.8 (830nm) was performed, followed by short-separation regression in HOMER3. The long separation channels (inter-optode distance of 30-40mm) measured the average change in the HbO2 from pre-task baseline at the task-relevant brain regions [8], including left PFC (LPFC), right PFC (RPFC), left PMC (LPMC), right PMC (RPMC), and SMA. The signal was found stationary for the 40s non-overlapping windows used for STFT.

D. Granger Causality Analysis

Consider two time-series, $X_1(t)$ and $X_2(t)$, where we assume each of these time series can be modeled by the combination of one another as expressed below:

$$X_1(t) = \sum_{i=1}^{n} a_i X_1(t-i) + \sum_{i=1}^{n} b_i X_2(t-i) + \epsilon_1(t) \quad (1)$$

$$X_2(t) = \sum_{i=1}^{n} c_i X_1(t-i) + \sum_{i=1}^{n} d_i X_2(t-i) + \epsilon_2(t) \quad (2)$$

where n is the order of the process. a, b, c and d are the coefficients, and $\epsilon(t)$ is the additive prediction error. If we introduce a lag operator, L^k, such that:

$$L^k X(t) = X(t-k)$$

then we can rewrite the equations (1) and (2) as:

$$X_1(t) = \left(\sum_{i=1}^{n} a_i L^i\right) X_1(t) + \left(\sum_{i=1}^{n} b_i L^i\right) X_2(t) + \epsilon_1(t) \quad (3)$$

$$X_2(t) = \left(\sum_{i=1}^{n} c_i L^i\right) X_1(t) + \left(\sum_{i=1}^{n} d_i L^i\right) X_2(t) + \epsilon_2(t) \quad (4)$$

Equations 3 and 4 can be arranged in a matrix form as:

$$\begin{pmatrix} a(L) & b(L) \\ c(L) & d(L) \end{pmatrix} \begin{pmatrix} X_1(t) \\ X_2(t) \end{pmatrix} = \begin{pmatrix} \epsilon_1(t) \\ \epsilon_2(t) \end{pmatrix} \quad (5)$$

To work in the frequency domain, we transform equation (5) using the Fast Fourier Transform (FFT) and get

$$\begin{pmatrix} a(\omega) & b(\omega) \\ c(\omega) & d(\omega) \end{pmatrix} \begin{pmatrix} X_1(\omega) \\ X_2(\omega) \end{pmatrix} = \begin{pmatrix} \epsilon_1(\omega) \\ \epsilon_2(\omega) \end{pmatrix} \quad (6)$$

where ω, is the frequency. We can rewrite equation 6 as:

$$\begin{pmatrix} X_1(\omega) \\ X_2(\omega) \end{pmatrix} = \begin{pmatrix} H_{11}(\omega) & H_{12}(\omega) \\ H_{21}(\omega) & H_{22}(\omega) \end{pmatrix} \begin{pmatrix} \epsilon_1(\omega) \\ \epsilon_2(\omega) \end{pmatrix} \quad (7)$$

where $\boldsymbol{H}$ is the transfer matrix.Then, GC can be found from the transfer matrix, $\boldsymbol{H}$, and the spectral matrix, $\boldsymbol{S}(\omega)$, that are related as follows [7]:

$$\boldsymbol{S}(\omega) = \boldsymbol{H}(\omega)\boldsymbol{\Sigma}(\omega)\boldsymbol{H}^*(\omega) \quad (8)$$

where * is the transposed conjugate operator. Here, the Wilson algorithm can factorize the spectral matrix, $\boldsymbol{S}(\omega)$, found from FFT:

$$\begin{bmatrix} S_{11}(\omega) & S_{12}(\omega) \\ S_{21}(\omega) & S_{22}(\omega) \end{bmatrix} = \begin{bmatrix} H_{11}(\omega) & H_{12}(\omega) \\ H_{21}(\omega) & H_{22}(\omega) \end{bmatrix} \begin{bmatrix} \Sigma_{11}(\omega) & \Sigma_{12}(\omega) \\ \Sigma_{21}(\omega) & \Sigma_{22}(\omega) \end{bmatrix} \begin{bmatrix} H^*{}_{11}(\omega) & H^*{}_{12}(\omega) \\ H^*{}_{21}(\omega) & H^*{}_{22}(\omega) \end{bmatrix}$$

However, if the $\sum_{12}(\omega) > 0$, then there is a third term resulting from the influence that correlated noise exerts on the spectra, which can be removed by the transformation introduced by Geweke [8], which we will use here (indicated by a tilde), see [7], [8] for details. Using Geweke's transformation and expanding the equation (8), the first term of $\boldsymbol{S}(\omega)$ can be written as:

$$S_{11}(\omega) = \widetilde{H}_{11}(\omega)\Sigma_{11}(\omega)\widetilde{H}^*_{11}(\omega) + H\widetilde{H}_{12}(\omega)\left(\Sigma_{22} - \frac{\Sigma_{12}^2}{\Sigma_{11}}\right)\widetilde{H}^*_{12}(\omega) \quad (9)$$

The first term of the equation (9) is the intrinsic term, and the second is the causal influence from X_2 to X_1 term [8]. So, the strict Granger causality for the frequency range from X_2 to X_1

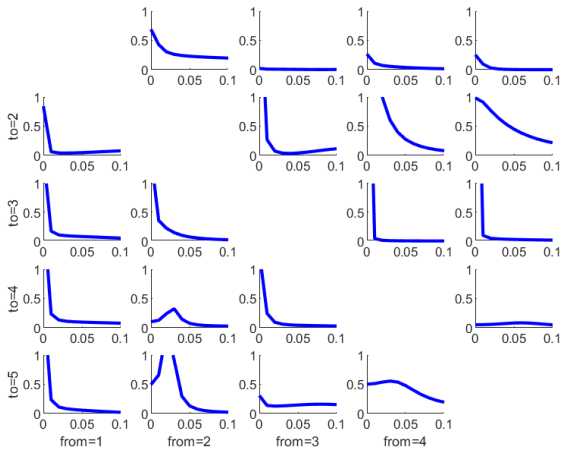

Fig. 1. Illustrative example of GC measured using STFFT. Each subplot represents the GC for each connection (depicted as from and to), the horizontal axis is the frequency axis and the vertical is the GC axis. The connecting number 1,2,3,4 and 5 corresponds to LPFC, RPFC, SMA, LPMC and RPMC respectively.

$(I_{2\to1})$ can be defined by dividing by the intrinsic term as follows:

$$I_{2\to1} = \log\left(\frac{S_{11}(\omega)}{\tilde{H}_{11}(\omega)\Sigma_{11}\tilde{H}^{*}{}_{11}(\omega)}\right) \quad (10)$$

Following similar steps, the Granger causality from X_1 to X_2 ($I_{1\to2}$) is expressed as:

$$I_{1\to2} = \log\left(\frac{S_{22}(\omega)}{\tilde{H}_{22}(\omega)\Sigma_{22}\tilde{H}^{*}{}_{22}(\omega)}\right) \quad (11)$$

This study has used Granger causality to estimate the linear causal relationship between each pair of the following brain regions: LPMC, RPMC, SMA, LPFC, and RPFC. To estimate the time-varying Granger causality, Short Time Fourier Transformation (STFT) was used. STFT is a sliding window method allowing to measure the GC over time. For this study, we selected non-overlapping 40 seconds time-windows based on the theoretical demonstration by Zalesky [9], and the STFT GC was computed using a Matlab toolbox [10] [11]. We selected the neurovascular coupling specific frequency band [0.01-0.07] Hz that avoids the systemic noise present outside of this frequency band. We averaged the GC in the neurovascular coupling frequency range [0.01 – 0.07] Hz. We then conducted statistical testing to compare the dynamic effective brain connectivity between the physical and the virtual simulators.

E. Statistical Testing

The GC strength for each forward and backward connections (i.e., LPFC→RPFC, LPFC→LPMC, LPFC→RPMC, LPFC→SMA, RPFC→LPFC, RPFC→LPMC, RPFC→RPMC, RPFC→SMA, LPMC→LPFC, LPMC→RPFC, LPMC→RPMC, LPMC→SMA, RPMC→LPFC, RPMC→RPFC, RPMC→LPMC, RPMC→SMA, SMA→LPFC, SMA→RPFC, SMA→LPMC, SMA→RPMC) were used for statistical testing. We first used the Shapiro-Wilk normality test for each connection in both the cohorts. ANOVA parametric test or Wilcoxon rank sum non-parametric test compared inter-regional GC between the physical and virtual simulator group for significant difference ($p<0.05$).

III. Results

An illustrative example of inter-regional GC in the frequency range of [0-0.1] Hz is shown in the subplots of Fig. 1. Here, each subplot represents an inter-regional brain connection (N = 20). Then, the GC's average in the frequency band of [0.01-0.07]Hz for each inter-regional brain connection is shown in figure (2). The normality test showed that most of the GC measures satisfied normal distribution for all the windows in both the cohorts. ANOVA found a statistically significant ($p <0.05$) difference in LPMC→ RPMC inter-regional brain connection between physical and virtual simulator in the first time window, which is shown in table (I). Moreover, LPMC→ RPMC and RPMC→LPMC inter-regional brain connection showed alternating modulation during the latter part of the FLS PC task, as shown in Fig. 3.

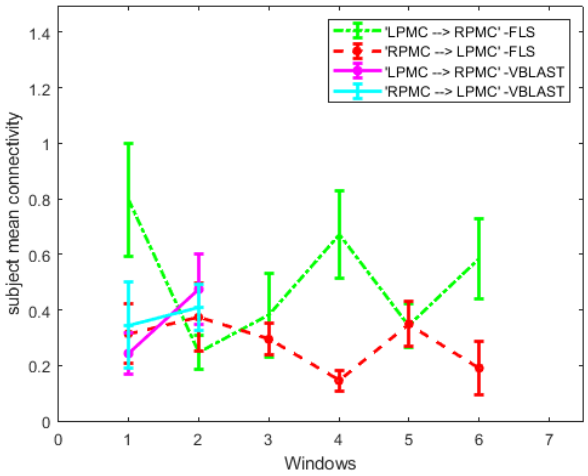

Fig. 3. Alternating change in the inter-regional directed brain connectivity (GC) between primary motor cortices

S.N.	Connection	window_1	window_2
1	LPFC→RPFC	0.381	0.094
2	LPFC→LPMC	0.968	0.339
3	LPFC→RPMC	0.067	0.793
4	LPFC→SMA	0.118	0.115
5	RPFC→LPFC	0.530	0.137
6	RPFC→LPMC	0.333	0.112
7	RPFC→RPMC	0.545	0.781
8	RPFC→SMA	0.303	0.138
9	LPMC→LPFC	0.396	0.872
10	LPMC→RPFC	0.583	0.527
11	LPMC-->RPMC	0.029	0.240
12	LPMC-->SMA	0.717	0.985
13	RPMC-->LPFC	0.524	0.148
14	RPMC-->RPFC	0.607	0.529
15	RPMC-->LPMC	0.887	0.207
16	RPMC-->SMA	0.239	0.127
17	SMA-->LPFC	0.859	0.086

18	SMA-->RPFC	0.671	0.163
19	SMA-->LPMC	0.685	0.847
20	SMA-->RPMC	0.628	0.424

Table 1: p-values from the analysis of variance of each inter-regional brain connection to compare between the physical and virtual simulator

IV. Discussion

In this study, we focused on five brain regions that are considered to directly associate with FLS PC tasks based on our prior work [2]. We found that the inter-regional directed brain connectivity (GC) of LPMC → RPMC was different ($p < 0.05$) at the start of the FLS PC task for the novice medical students trained on the physical simulator when compared to those compared to training on a virtual simulator. This aligned well with our prior work using magnitude-squared wavelet coherence *(in press)*[12] that showed inter-regional brain connectivity between the primary motor cortices to be distinguishing between training in the physical versus virtual simulator. Here, the left hemisphere is the dominant hemisphere in the right-handed subjects, so we postulate inter-hemispheric inhibition (IHI) from LPMC to RPMC at the beginning of the FLC PC task that is signifzicantly different between the physical and virtual simulator training.

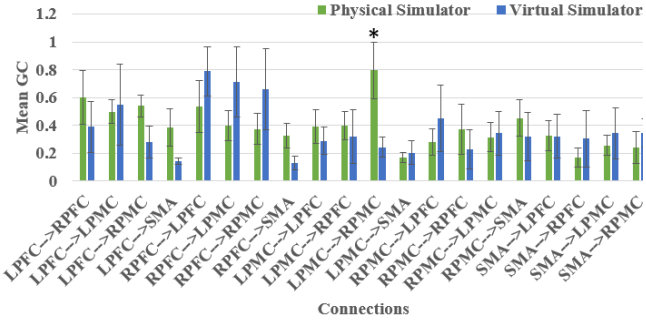

Fig. 2. Mean GC with standard error bar for the first window of the physical and virtual simulator.

Fig. 3 illustrates the alternating nature of LPMC → RPMC and RPMC → LPMC connectivity where the relationship between IHI, inter-hemispheric connectivity, and bimanual coordination during training performed in physical and virtual simulator needs neurophysiological investigation for simulator specificity [13].

Our results aligned well with the prior works using whole-brain imaging [14] that have demonstrated the necessity of the modulation of interhemispheric inhibition for bimanual coordination. However, his study has certain limitations, e.g., we did not perform an exhaustive search for optimal sliding window duration and stride in this study [15]. In the future, fNIRS based dynamic directed brain connectivity approach can be used for the brain-behavior investigation to assess and improve more complex bimanual laparoscopic surgical skills.

V. Conclusion

In this study, we conclude the following from our results,

- LPMC→RPMC effective brain connectivity distinguishes between physical and virtual surgical simulators at the start of the FLS PC task by the novice.
- LPMC→RPMC and RPMC→LPMC effective brain connectivity show alternating modulation at the latter part of the FLS PC task by the novice in both the physical and the virtual surgical simulators.

References

[1] A. Maciel, Y. Liu, W. Ahn, T. P. Singh, W. Dunnican, and S. De, "Development of the VBLaST™ : A virtual basic laparoscopic skill trainer," *Int. J. Med. Robot. Comput. Assist. Surg.*, 2008, doi: 10.1002/rcs.185.

[2] A. Nemani *et al.*, "Functional brain connectivity related to surgical skill dexterity in physical and virtual simulation environments," *Neurophotonics*, vol. 8, no. 01, Mar. 2021, doi: 10.1117/1.NPh.8.1.015008.

[3] D. P. Auer, "Spontaneous low-frequency blood oxygenation level-dependent fluctuations and functional connectivity analysis of the 'resting' brain," *Magn. Reson. Imaging*, vol. 26, no. 7, pp. 1055–1064, Sep. 2008, doi: 10.1016/j.mri.2008.05.008.

[4] M. Kamiński, M. Ding, W. A. Truccolo, and S. L. Bressler, "Evaluating causal relations in neural systems: Granger causality, directed transfer function and statist," *Biol. Cybern. 2001 852*, vol. 85, no. 2, pp. 145–157, 2001, doi: 10.1007/S004220000235.

[5] R. M. Hutchison *et al.*, "Dynamic functional connectivity: Promise, issues, and interpretations," *Neuroimage*, vol. 80, pp. 360–378, Oct. 2013, doi: 10.1016/j.neuroimage.2013.05.079.

[6] L. Hocke, I. Oni, C. Duszynski, A. Corrigan, B. Frederick, and J. Dunn, "Automated Processing of fNIRS Data—A Visual Guide to the Pitfalls and Consequences," *Algorithms*, vol. 11, no. 5, p. 67, May 2018, doi: 10.3390/a11050067.

[7] M. Dhamala, G. Rangarajan, and M. Ding, "Estimating granger causality from fourier and wavelet transforms of time series data," *Phys. Rev. Lett.*, vol. 100, no. 1, p. 018701, Jan. 2008, doi: 10.1103/PhysRevLett.100.018701.

[8] J. Geweke, "Measurement of linear dependence and feedback between multiple time series," *J. Am. Stat. Assoc.*, vol. 77, no. 378, pp. 304–313, 1982, doi: 10.1080/01621459.1982.10477803.

[9] A. Zalesky and M. Breakspear, "Towards a statistical test for functional connectivity dynamics," *NeuroImage*, vol. 114. Academic Press Inc., pp. 466–470, Jul. 01, 2015, doi: 10.1016/j.neuroimage.2015.03.047.

[10] J. Cui, L. Xu, S. L. Bressler, M. Ding, and H. Liang, "BSMART: A Matlab/C toolbox for analysis of multichannel neural time series," *Neural Networks*, vol. 21, no. 8, pp. 1094–1104, Oct. 2008, doi: 10.1016/j.neunet.2008.05.007.

[11] L. Barnett and A. K. Seth, "The MVGC multivariate Granger causality toolbox: A new approach to Granger-causal inference," *J. Neurosci. Methods*, vol. 223, pp. 50–68, Feb. 2014, doi: 10.1016/j.jneumeth.2013.10.018.

[12] A. Dutta, A. Kamat, B. Makled, J. Norfleet, X. Intes, and S.-V. De, "Interhemispheric functional connectivity in the primary motor cortex distinguishes between training on a physical and a virtual surgical simulator," doi: 10.1101/2021.07.10.451831.

[13] Y.-L. Kuo and B. E. Fisher, "Relationship between interhemispheric inhibition and bimanual coordination: absence of instrument specificity on motor performance in professional musicians," *Exp. Brain Res.*, vol. 238, no. 12, pp. 2921–2930, Dec. 2020, doi: 10.1007/s00221-020-05951-3.

[14] P. Bahrami *et al.*, "Neuroanatomical correlates of laparoscopic surgery training," *Surg. Endosc.*, vol. 28, no. 7, pp. 2189–2198, Feb. 2014, doi: 10.1007/s00464-014-3452-7.

[15] Z. Wang *et al.*, "Best window width determination and glioma analysis application of dynamic brain network measure on resting-state functional magnetic resonance imaging," *J. Med. Imaging Heal. Informatics*, vol. 6, no. 7, pp. 1735–1740, Nov. 2016, doi: 10.1166/jmihi.2016.1881.